International Journal of Science and Research (IJSR)
ISSN (Online): 2319-7064
Index Copernicus Value (2013): 6.14 | Impact Factor (2013): 4.438

Finite Element Analysis of Friction Welding Process for 2024Al Alloy and AISI 1021 Steel

T. Santhosh Kumar[1], A. Chennakesava Reddy[2]

[1]PG student, Department of Mechanical Engineering, JNTUH College of Engineering, Kukatpally, Hyderabad – 500 085, Telangana, India

[2]Professor, Department of Mechanical Engineering, JNTUH College of Engineering, Kukatpally, Hyderabad – 500 085, Telangana, India

Abstract: ***The purpose of this work was to weld dissimilar metals of 2024Al and AISI 1021 steel by continuous drive friction welding. The finite element analysis has been carried out to model the continuous drive friction welding. The process parameters have been optimized using Taguchi techniques. The optimal process parameters for 2024Al and AISI 1021 steel are found to be frictional pressure of 35 MPa, frictional time of 3 sec, rotational speed of 1500 rpm and forging pressure of 37.5 MPa.***

Keywords: 2024Al, AISI 1021 Steel, finite element analysis, Taguchi, continuous drive friction welding.

1. Introduction

Friction welding is a solid-state welding process that allows material combinations to be joined than with any other welding process. In continuous drive friction welding, one of the workpieces is attached to a motor driven unit while the other is restrained from rotation as showed in figure 1a. The motor driven workpiece is rotated at a predetermined constant speed. The workpieces to be welded are forced together and then a friction force is applied as shown in figure 1b. Heat is generated because of friction between the welding surfaces. This is continued for a predetermined time as showed in figure 1c. The rotating workpiece is halted by the application of a braking force. The friction force is preserved or increased for a predetermined time after the rotation is ceased (figure1d). Figure1also illustrates the variation of welding speed, friction force and forging force with time during various stages of the friction welding process.

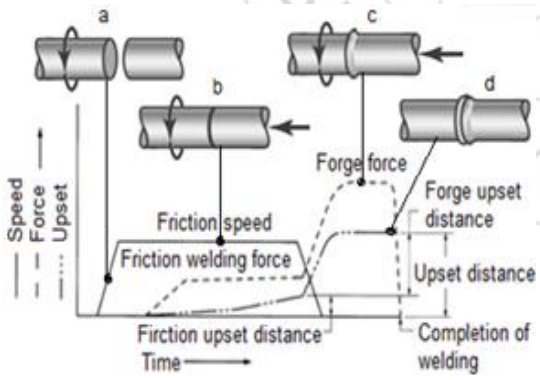

Figure 1: Friction welding

Even metal combinations not normally considered compatible can be joined by friction welding, such as aluminum to steel, copper to aluminum, titanium to copper and nickel alloys to steel. As a rule, all metallic engineering materials which are forgeable can be friction welded, including automotive valve alloys, maraging steel, tool steel, alloy steels and tantalum [1, 2]. With friction welding, joints are possible between not only two solid materials or two hollow parts, but also solid material/hollow part combinations can be reliably welded. However, the shape of a fusion zone in friction welding is dependent the force applied and the rotational speed. If the applied force is too high or the rotational speed is too low, the fusion zone at the centre of the joint will be narrow as showed in figure 2a. On the other hand, if the applied force is too low or the rotational speed is too high, the fusion zone at the centre of the joint will be wider as showed in figure 2b. In both the cases, the result is poor weld joint strength.

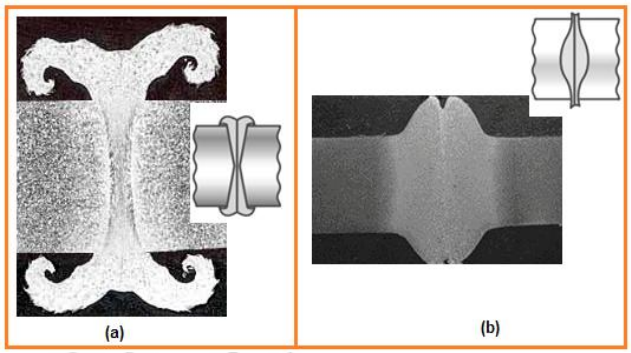

Figure 2: Effect of force and rotational speed in friction welding

In the friction welding process, the developed heat at the interface raises the temperature of work pieces rapidly to values approaching the melting range of the material. Welding occurs under the influence of pressure that is applied when heated zone is in the plastic range, as mentioned [3]. The foremost difference between the welding of similar materials and that of dissimilar materials is that the axial movement is unequal in the latter case whilst the similar materials experience equal movement along the common axis. This problem arises not only from the different coefficients of thermal expansion, but also from the distinct hardness values of the dissimilar materials to be joined. Joint and edge preparation is very important to produce distortion free welds. The solid-state diffusion is slow in the wider joints [4].The intermetallic compounds can change the micro hardness near the joint interface of dissimilar metals [5].

The difficulties in the welding of 2024 aluminum alloy with AISI 1021 steel by fusion welding processes have been a great challenge for engineering; because they result from hard and brittle inter metallic phases that formed between

aluminum and steel at evaluated temperatures. Therefore, friction welding of these materials needs to be eased by ensuring that both the workpieces deform similarly. In this context, this research work aims at finite element analysis of friction welding process for aluminum (2024Al) alloy and AISI 1021 steel.

2. Finite Element Modeling

In this study, ANSYS workbench (15.0) software was used in the coupled deformation and heat flow analysis during friction welding of AISI 1021 Steel and aluminum (2024Al) alloy. An axisymmetric 3D model [6] of aluminum (2024A) - AISI 1021 Steel rods of 25.4 mm diameter and 100 mm length was made using ANSYS workbench as shown in figure 3. Hexahedron elements [7] were used to mesh the aluminum and AISI 1021 Steel rods. The rotating part was modeled with 3298 elements and 14904 nodes and the non-rotating part was meshed with 16493 nodes and 3672 elements.

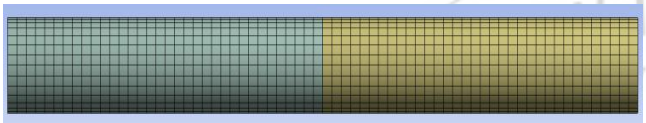

Figure 3: Finite element modeling of friction welding

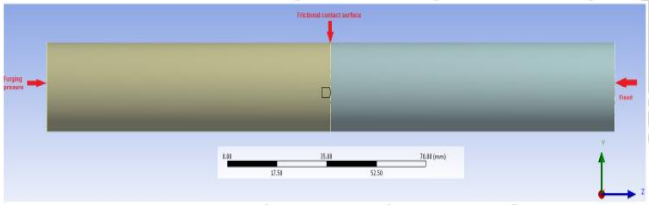

Figure 4: The boundary conditions

The boundary conditions are mentioned in figure 4. First the transient thermal analysis was carried out keeping AISI 1021 Steel rod stationary and aluminum rod in rotation. The coefficient of friction 0.2 was applied at the interface of AISI 1021 Steel rod and aluminum rods. The convection heat transfer coefficient was applied on the surfaces of two rods. The heat flux calculations were imported from ANSYS APDL commands and applied at the interface. The temperature distribution was evaluated. The thermal analysis was coupled to static structural analysis. For the structural analysis the rotating (aluminum) rod was brought to stationary and the forging pressure was applied on the AISI 1021 Steel rod along the axis of rod. The AISI 1021 Steel rod was allowed to move in the axial direction. The structural analysis was carried out for the equivalent stress and strain, total and directional deformation. The contact analysis was also carried out to estimate the depth of penetration and sliding of the material at the interface.

Table 1: Process parameters and levels

Factor	Symbol	Level–1	Level–2	Level–3
Frictional Pressure, MPa	A	25	30	35
Frictional time, Sec	B	3	4	5
Rotational speed	C	1000	1250	1500
Forging pressure, MPa	D	31.25	37.5	43.75

The analysis of friction welding was carried out as per the design of experiments using Taguchi techniques. The process parameters and their levels are given table-1. The orthogonal array (OA), L9 was selected for the present work. The parameters were assigned to the various columns of O.A. The assignment of parameters along with the OA matrix is given in Table 2.

Table 2: Orthogonal Array (L9) and control parameters

Treat No. No.	A	B	C	D
1	1	1	1	1
2	1	2	2	2
3	1	3	3	3
4	2	1	2	3
5	2	2	3	1
6	2	3	1	2
7	3	1	3	2
8	3	2	1	3
9	3	3	2	1

3. Results and Discussion

The temperature distribution from the transient thermal analysis; equivalent stress and directional deformation from the structural analysis; penetration and sliding from the contact analysis are discussed in the following sections.

Table 3: ANOVA summary of the temperature distribution

Source	Sum 1	Sum 2	Sum 3	*SS*	*v*	*V*	*F*	*P*
A	2683	3192	3616	72708	2	36354.06	12800.73	32.97
B	2994	2729	3768	97198	2	48599.21	17112.4	44.07
C	2863	3330	3298	22709	2	11354.79	3998.16	10.29
D	2843	3406	3241	27907	4	6976.81	2456.62	12.65
e				20	7	2.84	1	0.02
T	11384	12658	13924	220543	17			100

Note: SS is the sum of square, v is the degrees of freedom, V is the variance, F is the Fisher's ratio, P is the percentage of contribution and T is the sum squares due to total variation.

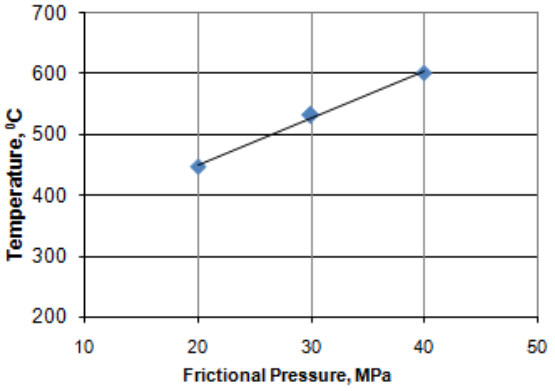

Figure 5: Influence of frictional pressure on temperature.

3.1 Influence of parameters on temperature distribution

Table – 3 gives the ANOVA (analysis of variation) summary of raw data. The Fisher's test column establishes all the parameters (A, B, C and D) accepted at 90% confidence level. The percent contribution indicates that the friction pressure, A contributes 32.97% of variation, B (friction time) aids 44.07% of variation, C (rotational speed) influences 10.29% of variation and D (forging pressure) contributes 12.65% of

variation on the temperature distribution. The effect of forging pressure is due to reaction of frictional pressure.

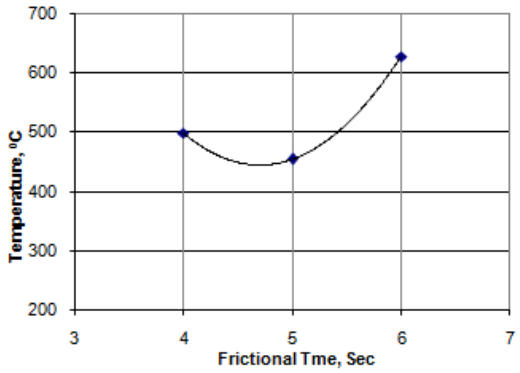

Figure 6: Influence of frictional time on temperature.

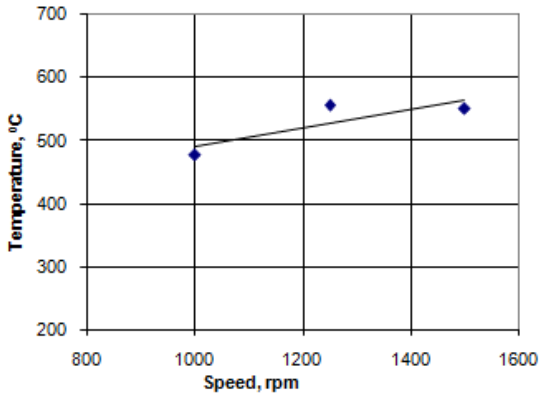

Figure 7: Influence of rotational speed on temperature.

The temperature developed in the welding rods is directly proportional to the frictional pressure, rotational speed and forging pressure as shown in figure 5, 7 & 8. In fact this is natural phenomena. The effect of frictional time on the generation of temperature is polynomial as shown in figure 6. Form figure 9 it is observed that the temperature is very high at the interface. The trial 9 gives the highest temperature generation and trial 1 gives the lowest temperature generation in the rods. Change of temperature field is generated by heat flux that depends on: frictional pressure on the contact surface, relative velocity of the two faces, frictional time and coefficient of friction.

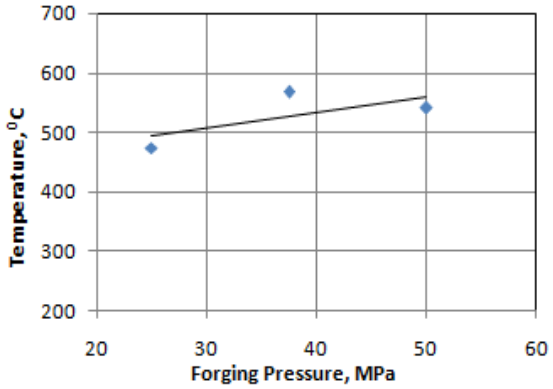

Figure 8: Influence of forging pressure on temperature.

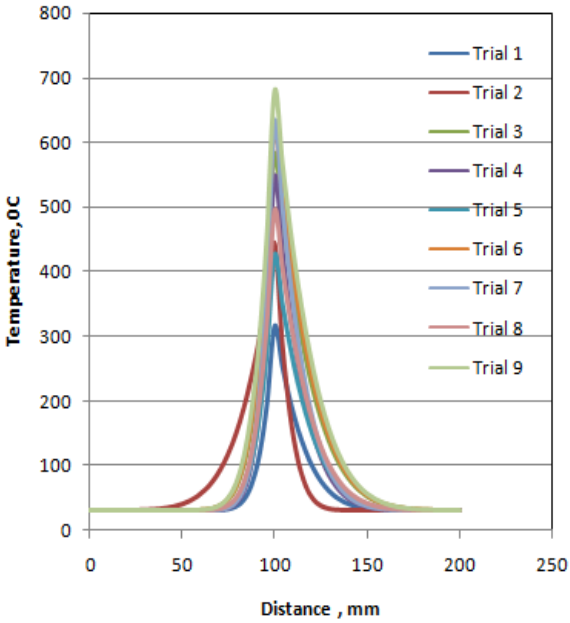

Figure 9: Temperature distribution during different trials

3.2 Influence of parameters on equivalent stress

The ANOVA summary of the elastic modulus is given in Table 4. The Fisher's test column ascertains all the parameters (A, B, C, D) accepted at 90% confidence level influencing the variation in the equivalent stress. The contribution of friction pressure, frictional time, rotational speed and forging pressure are 43.74%, 26.21%, 12.97%, and 16.96% respectively towards variation in the effective stress.

Table 4: ANOVA summary of the equivalent stress

Source	Sum 1	Sum 2	Sum 3	*SS*	*v*	*V*	*F*	*P*
A	957.578	1190.19	1369.03	14188.05	2	7094.025	3135.38	43.74
B	1314.43	999.43	1202.93	8503.4	2	4251.7	1879.14	26.21
C	1042.95	1227.47	1246.38	4210.46	2	2105.23	930.46	12.97
D	1028.25	1275.36	1213.19	5507.22	4	1376.80	608.51	16.96
e				15.84	7	2.26	1.00	0.12
T	4343.21	4692.45	5031.53	32424.97	17			100

The equivalent stress increases with an increase in the frictional pressure, rotational speed and forging pressure as shown in figure 10, 12 & 13. The effect of frictional time is polynomial on the equivalent stress (figure 11). The equivalent stress is low for the frictional time of 5 sec.

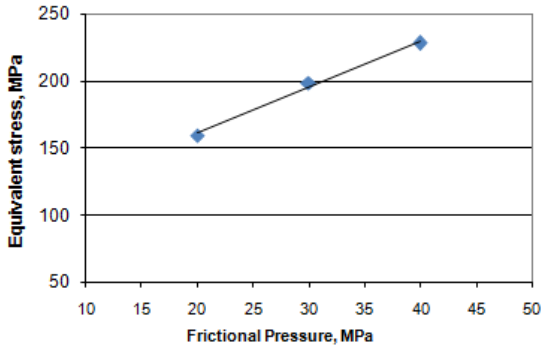

Figure 10: Influence of frictional pressure on equivalent stress.

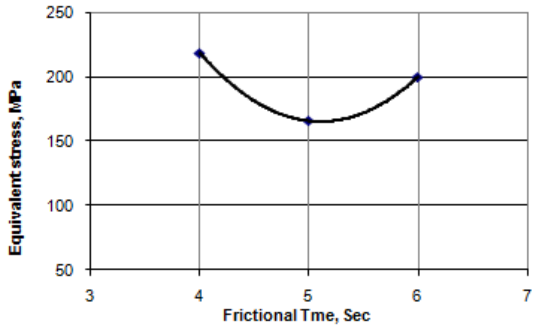

Figure 11: Influence of frictional time on equivalent stress.

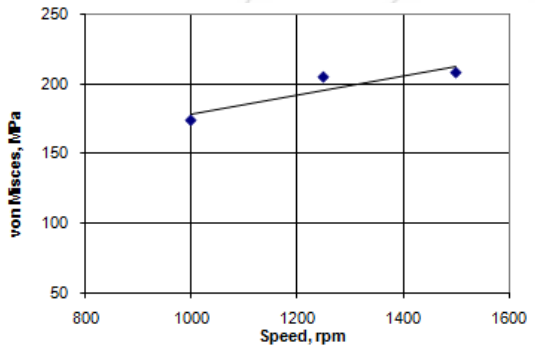

Figure 12: Influence of rotational speed on equivalent stress.

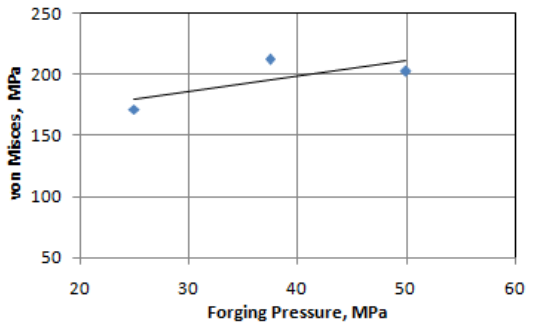

Figure 13: Influence of forging pressure on equivalent stress.

It is observed from table 5 that the equivalent stress is 280.53 MPa for trail 7 at the end of frictional heating and is 154.27 MPa at the end of forging pressure. It is also observed from table 5 that the equivalent stress is 138.16 MPa for trail 1 at the end of frictional heating and is 87.31 MPa at the end of forging pressure. During friction heating stage any surface irregularities are removed, the temperature increases in the vicinity of the welded surfaces, and an interface of visco-plastic aluminum is formed. During forging pressure stage there is significant thermo-plastic deformation of aluminum in the contact area. In result of this is formation of a flange-like flash. The process of welding takes place due to the plastic and diffusion effects.

3.3 Influence of parameters on total deformation

The ANOVA summary of the directional deformation is given in Table 6. The Fisher's test column ascertains all the parameters (A, B, C, D) accepted at 90% confidence level influencing the variation in the directional deformation. The major contribution (38.18%) is of frictional pressure and frictional time towards variation in the directional deformation. The influence of rotational speed and forging pressure are 26.20% and 16.45% respectively.

Table 5: Equivalent stress values under different trials

	At end of frictional heating	At end of forging
1	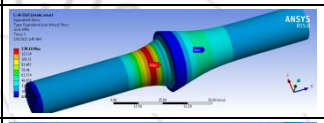	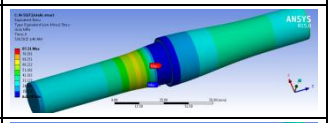
2	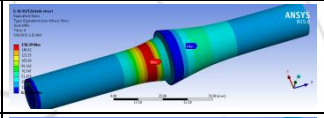	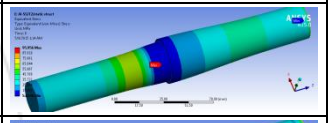
3	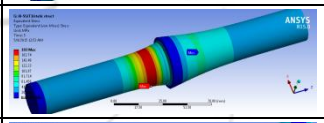	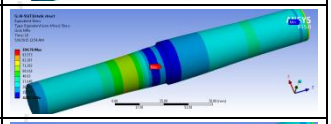
4	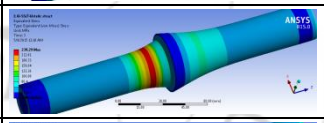	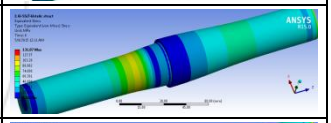
5	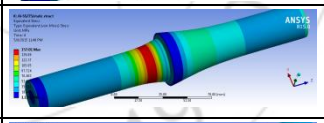	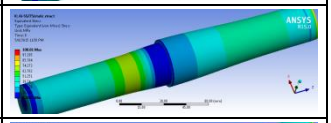
6	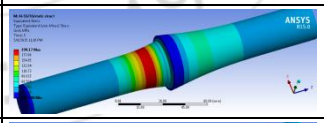	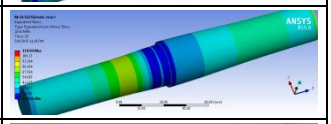
7	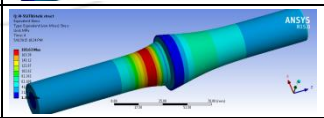	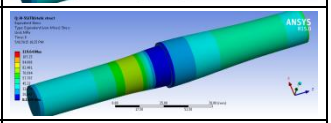
8	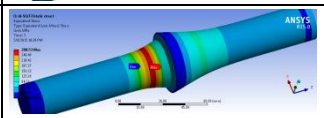	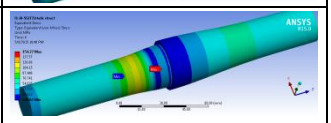
9	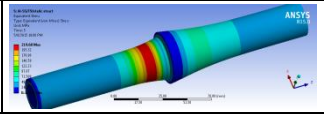	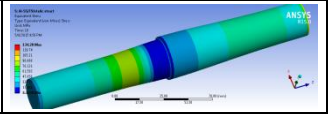

Table 6: ANOVA summary of the directional deformation

Source	Sum 1	Sum 2	Sum 3	*SS*	*v*	*V*	*F*	*P*
A	1.1096	1.37368	1.45283	0.01	2	0.005	12.30	12.61
B	1.0884	1.0814	1.76634	0.05	2	0.025	61.50	67.52
C	1.1571	1.41152	1.36744	0	2	0	0.00	-1.12
D	1.1946	1.38833	1.35314	0.01	4	0.0025	6.15	11.5
e				0.002845	7	0.000406	1.00	9.49
T	4.54973	5.25493	5.93975	0.072845	17			100

The total deformation increases with an increase in the frictional pressure, frictional time and forging pressure as shown in figure 14, 15 & 16. In the first numerical iteration (thermal) the external load generates uniform pressure on the contact surface and consequently linearly changing heat flux. There is a gap between steel aluminum as seen from table 6. In the next iteration (static) the forging pressure on the contact surface forces the material to penetrate and slid. There is no gap between steel aluminum. The extruded shape gradually forms near the welded joint during the welding process. The extruded shape is asymmetric, as shown in table 6. It results from non-uniform material properties along the radial direction of the specimen during welding.

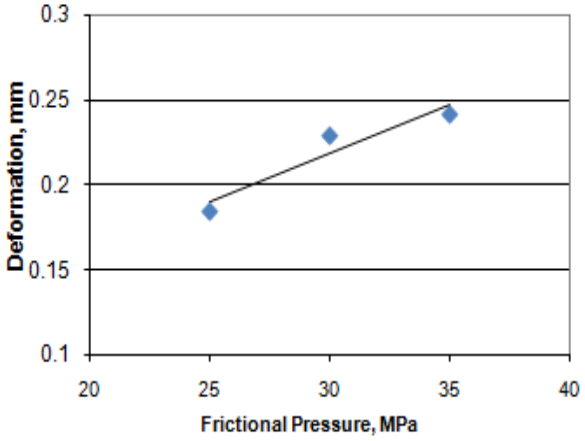

Figure 14: Influence of frictional pressure on deformation

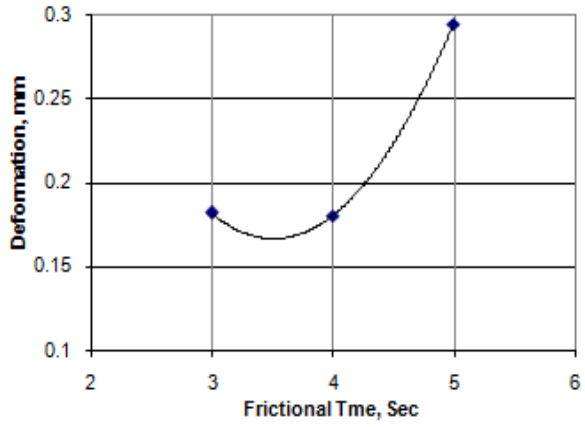

Figure 15: Influence of frictional time on deformation

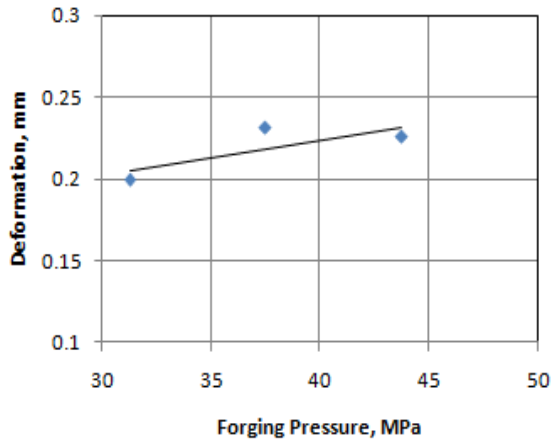

Figure 16: Influence of forging pressure on deformation

3.4 Influence of parameters on penetration and sliding

In friction welding of 2024Al and AISI 1021 Steel, only 2024Al is consumed in the form of flash due to softer and high thermal conductive material as most of the heat generated at the interface is transferred to 2024Al. The deformation of AISI 1021 Steel is negligible due to its higher hardness value, and higher melting point as shown in table 7. In the case of trail 1 the interface layer has not produced a good metallic bond between aluminum and AISI 1021 Steel. In the case of trail 4 and 7 the interface layer has produced a good metallic bond between aluminum and steel. The penetrations of trails 4 and 7 are 0.0017 and 0.002 mm respectively. A closer look at the penetration and sliding images shows that the failure of good bonding has taken place largely by interface separation. One factor may be the uneven rate of heat generation. Due to this uneven rate of heat input, the amount of melt-off for each cycle for welding this combination of steel and aluminum.

Table 6: Directional deformation values under different trials

	At end of frictional heating	At end of forging
1	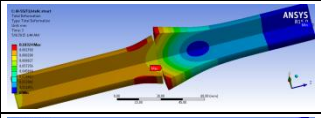	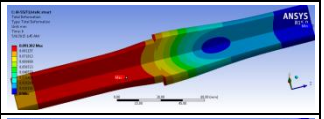
2	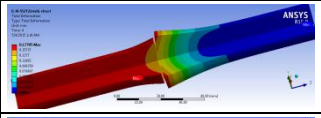	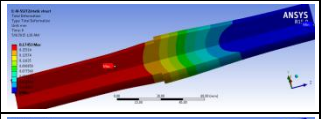
3	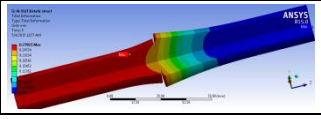	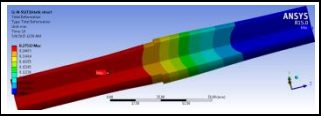

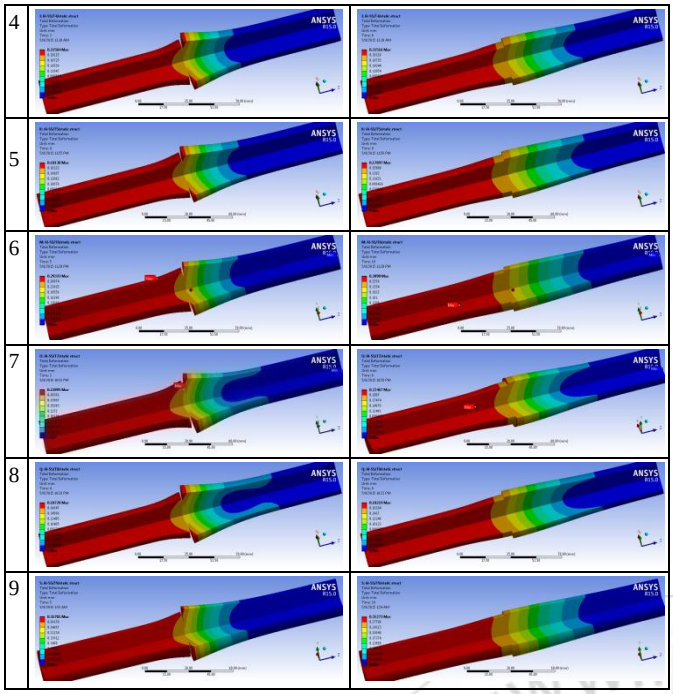

The optimal process parameters for 2024Al and AISI 1021 Steel are found to be frictional pressure of 35 MPa, frictional time of 3 sec, rotational speed of 1500 rpm and forging pressure of 37.5 MPa. For this dissimilar metals of aluminium and steel, the forging pressure should be higher than the frictional pressure. The experimental fricitional welding validateds the the seventh trial conditions as shown in figure 17.

4. Conclusions

This study shows that the 2024Al and AISI 1021 Steel is good if the operating conditions: frictional pressure of 35 MPa, frictional time of 3 sec, rotational speed of 1500 rpm and forging pressure of 37.5 MPa. For friction welding of AISI 1021 Steel and aluminum the forging pressure should be less than the frictional pressure or equal. For this condition of welding there was good penetration and sliding of materials at the welding interface resulting a good mechanical bonding.

Table 7: Sliding and penetration values under different trials

	Sliding	Penetration
1		
2		
3		
4		

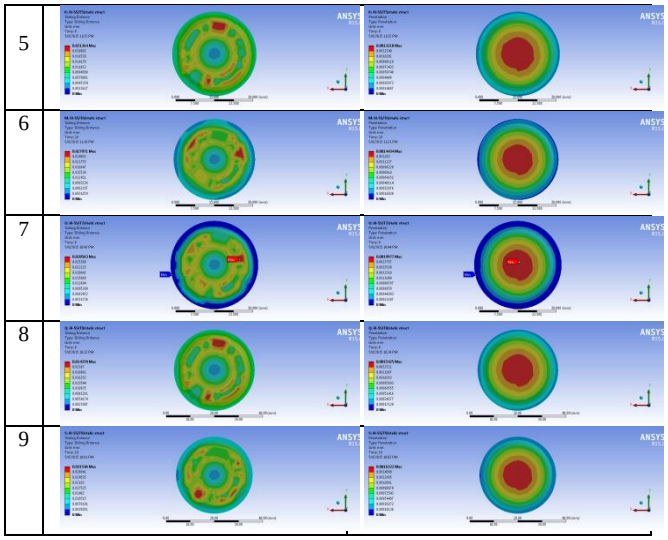

Figure 17: Welding 2024 Al alloy and AISI 1021 steel with trial 7 conditions

5. Acknowledgements

The author acknowledges with thanks University Grants Commission (UGC) – New Delhi for sectioning R&D project.

References

[1] A. Chennakesava Reddy, Fatigue Life Evaluation of Joint Designs for Friction Welding of Mild Steel and Austenite Stainless Steel, International Journal of Science and Research, vol.4, n0.2, pp. 1714-1719, 2015.
[2] A. Chennakesava Reddy, Fatigue Life Prediction of Different Joint Designs for Friction Welding of 1050 Mild Steel and 1050 Aluminum, International Journal of Scientific & Engineering Research, vol.6, no.4, pp. 408-412, 2015.
[3] B.S. Yibas, A.Z. Sahin, N. Kahrama, and A.Z. Al-Garni, "Friction welding of St-A1 and A1-Cu materials", Journal of Materials Processing Technology", (49), pp.431-443, 1995.
[4] A. Chennakesava Reddy, A. Ravaivarma, and V. Thirupathi Reddy, in Proceedings of National Welding Seminar, IIT-Madras, pp.51-55, 2002.
[5] W. Li and F. Wang, "Modeling of continuous drive friction welding of mild steel", Materials Science and Engineering A, (528), pp.5921-5926, 2011.
[6] Chennakesava, R. Alavala, "CAD/CAM: Concepts and Applications," PHI Learning Pvt. Ltd, 2008:
[7] Chennakesava R. Alavala, "Finite element methods: Basic Concepts and Applications, PHI Learning Pvt. Ltd., 2009.